Chapter 4

On singularly perturbed delay Volterra integro-differential equations[3]

In this chapter, we examine the following linear singularly perturbed delay Volterra integro-differential equations (SPDVIDEs)

$$\begin{cases} \mathscr{L}u := \varepsilon u'(t) + a(t)u(t) + b(t)u(t-r) \\ \qquad + \displaystyle\int_0^t \left[K(t,s)\,u(s) + L(t,s)\,u(s-r)\right] ds = f(t), \quad t \in \mathfrak{I} = (0,T], \end{cases} \tag{4.1}$$

$$u(t) = \psi(t), \quad t \in \mathfrak{I}_0 = [-r, 0], \tag{4.2}$$

where $\varepsilon \in (0,1]$ is the 'perturbation parameter', $\mathfrak{I} = \cup_{q=1}^{m} \mathfrak{I}_q$, $\mathfrak{I}_q = \{t : r_{q-1} < t \le r_q\}$ for $1 \le q \le m$ with $r_p = pr$, $0 \le p \le m$, and r is a constant delay. For simplicity, we assume that p, q and m are integers, i.e. $T = mr$. Further, $a(t) \ge \delta > 0$, $b(t), f(t)\,(t \in \bar{\mathfrak{I}}), \psi(t)\,(t \in \mathfrak{I}_0), K(t,s)$ and $L(t,s)\,((t,s) \in \bar{\mathfrak{I}} \times \bar{\mathfrak{I}})$ are supposed to be sufficiently smooth functions. With these assumptions, SPDVIDE (4.1)–(4.2) has a unique solution (see [103]). Further, it has boundary layers on the right side of each point $t = r_q\,(0 \le q \le m-1)$ for small values of ε. The occurrence of multiple boundary layers is due to the presence of delay term r in the governing problem.

Singularly perturbed Volterra integro-differential equations without delay exhibit only a single layer at $t = 0$. Contrastingly, SPDVIDE (4.1)–(4.2) possess multiple boundary layers, which makes the construction of numerical methods and analysis

[3]This chapter contains material published in *Numerical Algorithms*, 2023, doi: `https://doi.org/10.1007/s11075-023-01620-y`.

quite difficult. Further, note that not all singularly perturbed delay Volterra integro-differential equations possess multiple boundary layers (see, e.g. [115]). So, one has to be very careful while dealing with singularly perturbed delay Volterra integro-differential equations.

Note that the work of [103] is restricted to Shishkin meshes only. Hence, for SPDVIDE (4.1)–(4.2), it is interesting to develop a framework based on which all a priori meshes of Shishkin and Bakhvalov type can be analyzed. It is noteworthy to mention that Bakhvalov type meshes produce results superior than Shishkin type meshes, because with Bakhvalov type meshes logarithmic factor does not appear in the error bound, which is in contrast to Shishkin type meshes. Further, it is also interesting to derive the a posteriori error estimate for SPDVIDE (4.1)–(4.2) based on which the a posteriori meshes can be constructed. So, the present work intends to fill these gaps in the literature.

We discretize SPDVIDE (4.1)–(4.2) by an implicit difference scheme for the derivative term and a composite numerical integration rule for the integral terms. The analysis of the discrete scheme consists of two parts and involves more technical arguments than the analysis of singularly perturbed Volterra integro-differential equations without delay. First, we establish an a priori error estimate that is used to prove robust convergence of the discrete scheme on Shishkin and Bakhvalov type meshes, whereas [103] is limited to Shishkin meshes. Next, we establish the maximum norm a posteriori error estimate that involves difference derivatives of the approximate solution. The derived a posteriori error estimate gives the computable and guaranteed upper bound on the error. It is advantageous in the sense that an adaptive mesh for SPDVIDE (4.1)–(4.2) can be automatically generated using the derived a posteriori error estimate.

The arrangement of this chapter is as follows. In Section 4.1, we describe the stability bound for SPDVIDE (4.1)–(4.2). The discretization for the considered problem is given in Section 4.2. We establish the a priori error estimate in Section 4.3, while the a posteriori error estimation is given in Section 4.4. Numerical results in the form of tables and graphs are included in Section 4.5. Finally, some concluding remark is given in Section 4.6.

4.1 Stability of SPDVIDE

In what follows, we will frequently use the following notations. For any function V, $\|V\|_\infty$ represents the maximum norm on $\bar{\mathcal{I}}$. Further, we shall denote $\|V\|_{\infty,q} = \|V\|_{\infty,\bar{\mathcal{I}}_q} = \sup_{t\in\bar{\mathcal{I}}_q}|V(t)|, 0 \le q \le m$. Also, we define $\bar{\mathcal{I}}$ as the closure of the interval $\mathcal{I}$, $\bar{K} = \max_{\bar{\mathcal{I}}\times\bar{\mathcal{I}}}|K(t,s)|$, $\bar{K}_t = \max_{\bar{\mathcal{I}}\times\bar{\mathcal{I}}}|K_t(t,s)|$, $\bar{K}_s = \max_{\bar{\mathcal{I}}\times\bar{\mathcal{I}}}|K_s(t,s)|$, $\bar{L} = \max_{\bar{\mathcal{I}}\times\bar{\mathcal{I}}}|L(t,s)|$, and $\bar{L}_t = \max_{\bar{\mathcal{I}}\times\bar{\mathcal{I}}}|L_t(t,s)|$, $\bar{L}_s = \max_{\bar{\mathcal{I}}\times\bar{\mathcal{I}}}|L_s(t,s)|$. Here, $K_t(t,s) = \dfrac{\partial}{\partial t}K(t,s)$, $K_s(t,s) = \dfrac{\partial}{\partial s}K(t,s)$, $L_t(t,s) = \dfrac{\partial}{\partial t}L(t,s)$ and $L_s(t,s) = \dfrac{\partial}{\partial s}L(t,s)$.

Now, we discuss the stability and derivative estimates for the solution of SPDVIDE (4.1)–(4.2), which show the asymptotic characteristics of the solution and its first derivative.

Lemma 4.1. *The solution u of SPDVIDE (4.1)–(4.2) satisfies the following stability bound*

$$\begin{aligned}\|u\|_\infty \le & \|\psi\|_{\infty,0}\left(\delta^{-1}\|b\|_\infty e^{\frac{(\bar{K}+\bar{L})T}{\delta}}\right)^m + \left\{|\psi(0)| + \delta^{-1}\|f\|_\infty + \delta^{-1}\bar{L}\int_{-r}^{0}|\psi(t)|\,dt\right\} \\ & \cdot e^{\frac{(\bar{K}+\bar{L})T}{\delta}}\sum_{s=1}^{m}\left(\delta^{-1}\|b\|_\infty e^{\frac{(\bar{K}+\bar{L})T}{\delta}}\right)^{m-s} \qquad (4.3)\end{aligned}$$

Further, it holds

$$|u'(t)| \leq C\left\{1+\frac{(t-r_{q-1})^{q-1}}{\varepsilon^q}e^{-\frac{\delta(t-r_{q-1})}{\varepsilon}}\right\}, \quad t\in \bar{\mathfrak{I}}_q,\ 1\leq q\leq m. \tag{4.4}$$

Proof. The proof follows using the arguments in [103, Lemma 2.2]. □

We next provide the corollary which will be useful in the a posteriori analysis given in Section 4.4.

Corollary 4.1. *Let $\mathscr{F}$ be any bounded piecewise continuous function such that*

$$\mathscr{L}u_1(t)-\mathscr{L}u_2(t)=\mathscr{F}(t),$$

for any two functions u_1 and u_2 satisfying $u_1(t)=u_2(t),\ t\in\mathfrak{I}_0$. Then, the following inequality holds

$$\|u_1-u_2\|_\infty \leq C_*\|\mathscr{L}u_1-\mathscr{L}u_2\|_\infty, \tag{4.5}$$

where $C_*=\delta^{-1}e^{\frac{(\bar{K}+\bar{L})T}{\delta}}\sum_{s=1}^{m}\left(\delta^{-1}\|b\|_\infty e^{\frac{(\bar{K}+\bar{L})T}{\delta}}\right)^{m-s}$.

Proof. For the simplicity, let $z=u_1-u_2$. Note that $\mathscr{L}z=\mathscr{L}(u_1-u_2)=\mathscr{L}u_1-\mathscr{L}u_2$. We have

$$\begin{cases}\mathscr{L}z=\varepsilon z'(t)+a(t)z(t)+b(t)z(t-r)+\displaystyle\int_0^t\left[K(t,s)\,z(s)+L(t,s)\,z(s-r)\right]ds\\ \qquad\ =\mathscr{F}(t), \qquad t\in(0,r_q],\\ z(t)=0, \qquad t\in\mathfrak{I}_0.\end{cases}$$

Clearly, the above problem is of the form of (4.1)–(4.2). Therefore, upon applying Lemma 4.1 to the above problem, we arrive at

$$\|z\|_\infty\leq C_*\|\mathscr{F}\|_\infty=C_*\|\mathscr{L}u_1-\mathscr{L}u_2\|_\infty.$$

□

4.2 Discretization

For the discretization of SPDVIDE (4.1)–(4.2), we consider an arbitrary non-uniform grid $\bar{\omega}_{N_0}$ on $\bar{\mathfrak{I}}$, defined as $\bar{\omega}_{N_0} \equiv \{0 = t_0 < t_1 < \cdots < t_{N_0-1} < t_{N_0} = T\}$ with the grid size $h_i = t_i - t_{i-1}$ for $1 \leq i \leq N_0$. Note that $\bar{\omega}_{N_0}$ contains N grid points on each subinterval $\omega_{N,q}$ defined as

$$\omega_{N,q} = \{t_i : (q-1)N + 1 \leq i \leq qN\}, \quad 1 \leq q \leq m,$$

and consequently

$$\omega_{N_0} = \cup_{q=1}^{m} \omega_{N,q}.$$

Further, we define the discretization of $\mathfrak{I}_0$ as $\bar{\omega}_{N,0} = \{t_i : -N \leq i \leq 0\}$. Next, we define the backward Euler formula for any mesh function $\{V_i\}_{i=0}^{N_0}$ by

$$D^- V_i = \frac{V_i - V_{i-1}}{h_i}, \qquad 1 \leq i \leq N_0.$$

Integrating problem (4.1) over (t_{i-1}, t_i) and applying the composite right rectangle rule and then the composite left rectangle rule to the resulting integral term, we obtain the following difference approximation

$$\varepsilon D^- u_i + a_i u_i + b_i u_{i-N} + \sum_{j=0}^{i-1} h_{j+1} \left[K(t_i, t_j) u_j + L(t_i, t_j) u_{j-N}\right] + R_i = f_i, \ 1 \leq i \leq N_0 \quad (4.6)$$

with the remainder term

$$\mathcal{R}_i = \mathcal{R}_i^{(1)} + \mathcal{R}_i^{(2)} + \mathcal{R}_i^{(3)}, \quad (4.7)$$

where

$$\mathcal{R}_i^{(1)} = -h_i^{-1} \int_{t_{i-1}}^{t_i} (t - t_{i-1}) \frac{d}{dt} \left[a(t)u(t) + b(t)u(t-r) - f(t) \right] dt, \tag{4.8}$$

$$\mathcal{R}_i^{(2)} = -h_i^{-1} \int_{t_{i-1}}^{t_i} \left[(t - t_{i-1}) \frac{d}{dt} \int_0^t \left\{ K(t,s)u(s) + L(t,s)u(s-r) \right\} ds \right] dt, \tag{4.9}$$

$$\mathcal{R}_i^{(3)} = \sum_{j=1}^{i} \int_{t_{j-1}}^{t_j} (t_j - s) \frac{d}{ds} \left[K(t_i,s)u(s) + L(t_i,s)u(s-r) \right] ds. \tag{4.10}$$

Neglecting the truncation error $\mathcal{R}_i$ in (4.6), we finally have the following discrete scheme corresponding to the continuous problem (4.1)–(4.2):

$$\begin{cases} \mathscr{L}_N U_i := \varepsilon D^- U_i + a_i U_i + b_i U_{i-N} + \sum_{j=0}^{i-1} h_{j+1} \left[K(t_i,t_j)U_j + L(t_i,t_j)U_{j-N} \right] \\ \qquad\qquad = f_i, \quad i = 1, 2, \cdots, N_0, & (4.11) \\ U_i = \psi_i, \quad -N \le i \le 0, & (4.12) \end{cases}$$

where U_i is the approximation of $u(t_i)$.

4.3 A priori error analysis

To perform the a priori error analysis of the discrete scheme (4.11)–(4.12), we require the following stability bound.

Lemma 4.2. *For the solution U of (4.11)–(4.12), it holds*

$$\|U\|_{\bar{\omega}_{N_0}} \le C \left(\|\psi\|_{\bar{\omega}_{N,0}} + \|f\|_{\omega_{N_0}} \right).$$

Proof. The proof can be done using the ideas similar to the one in [103, Lemma 4.2]. □

We define the error function $\phi_i = U_i - u_i$ for $i = 1, 2, \cdots, N_0$. Observe that the error function ϕ satisfies the following discrete problem

$$\begin{cases} \mathscr{L}_N \phi_i = \mathcal{R}_i, \quad i = 1, 2, \cdots, N_0, & (4.13) \\ \phi_i = 0, \qquad i = -N, 1-N, \cdots, 0, & (4.14) \end{cases}$$

where the truncation error $\mathcal{R}_i$ is given by (4.7).

Before we proceed to establish our main *a priori* error bound, we define the following quantity that will be useful:

$$\vartheta_p(\omega) := \max_{1 \le q \le p} \max_{(q-1)N+1 \le j \le qN} \int_{t_{j-1}}^{t_j} \left\{ 1 + \frac{1}{\varepsilon} \exp\left(-\frac{\delta(s - r_{q-1})}{\theta \varepsilon} \right) \right\} ds, \quad 1 \le p \le m. \tag{4.15}$$

Theorem 4.1. *Let u be the solution of (4.1)–(4.2) and U be its approximation by the finite difference scheme (4.11)–(4.12). Then*

$$\|u - U\|_{\bar{\omega}_{N_0}} \le C \vartheta_m(\omega). \tag{4.16}$$

Proof. We begin the proof with the following estimate which we get after applying Lemma 4.2 to (4.13)–(4.14):

$$\|u - U\|_{\bar{\omega}_{N_0}} \le C \|\mathcal{R}\|_{\omega_{N_0}}. \tag{4.17}$$

Now, we have bound the truncation error $\mathcal{R}$. For the same we bound each part $\mathcal{R}^{(n)}, n = 1, 2, 3$, of the truncation error $\mathcal{R}$ separately. Using the stability estimate (4.3) in (4.8), we have

$$\left| \mathcal{R}_i^{(1)} \right| \le h_i^{-1} \int_{t_{i-1}}^{t_i} |(t - t_{i-1})| \left| \frac{d}{dt} [a(t)u(t) + b(t)u(t-r) - f(t)] \right| dt$$

$$\leq C \int_{t_{i-1}}^{t_i} (1 + |u'(t)| + |u'(t-r)|)\, dt. \tag{4.18}$$

Further, for the second part $\mathcal{R}_i^{(2)}$, (4.9) yields

$$\begin{aligned}
\left|\mathcal{R}_i^{(2)}\right| &\leq h_i^{-1} \int_{t_{i-1}}^{t_i} |(t - t_{i-1})| \left| \frac{d}{dt} \int_0^t \{K(t,s)u(t) + L(t,s)u(t-r)\}\, ds \right| dt \\
&\leq \int_{t_{i-1}}^{t_i} \left[|K(t,t)u(s) + L(t,t)u(s-r)| + \left| \int_0^t \frac{\partial}{\partial t} \Big(k(t,s)u(s) + L(t,s)u(s-r) \Big) ds \right| \right] dt \\
&\leq C \int_{t_{i-1}}^{t_i} dt,
\end{aligned} \tag{4.19}$$

where the Leibnitz rule and smoothness conditions on K and L are utilized. Next, we bound the third part $\mathcal{R}_i^{(3)}$ using (4.10) as follows

$$\begin{aligned}
\left|\mathcal{R}_i^{(3)}\right| &\leq \left| \sum_{j=1}^{i} \int_{t_{j-1}}^{t_j} (t_j - s) \frac{d}{ds} \Big(K(t_i,s)u(s) + L(t_i,s)u(s-r) \Big)\, ds \right| \\
&\leq \sum_{j=1}^{i} \int_{t_{j-1}}^{t_j} |(t_j - s)| \left| \frac{\partial}{\partial s} K(t_i,s)u(s) + \frac{\partial}{\partial s} L(t_i,s)u(s-r) \right. \\
&\qquad \left. + K(t_i,s)u'(s) + L(t_i,s)u'(s-r) \right| ds \\
&\leq C \sum_{j=1}^{i} h_j \int_{t_{j-1}}^{t_j} (|1 + u'(s) + u'(s-r)|) ds \\
&\leq C \left(\max_{1 \leq j \leq i} \int_{t_{j-1}}^{t_j} (1 + |u'(s)| + |u'(s-r)|) ds \right) \left(\sum_{j=1}^{i} h_j \right) \\
&\leq C \max_{1 \leq j \leq i} \int_{t_{j-1}}^{t_j} (1 + |u'(s)| + |u'(s-r)|) ds,
\end{aligned} \tag{4.20}$$

where (4.3) is taken into account. Hereby, combining the bounds (4.18)–(4.20), we get

$$|\mathcal{R}_i| \leq C \max_{1 \leq j \leq i} \int_{t_{j-1}}^{t_j} (1 + |u'(s)| + |u'(s-r)|) ds. \tag{4.21}$$

We proceed further by considering two different cases, viz. for mesh points lying in $\omega_{N,1}$ and $\omega_{N,p}$, $1 < p \leq m$. For the first case, i.e. on $\omega_{N,1}$, (4.21) and Lemma 4.1

gives

$$\|\mathcal{R}\|_{\omega_{N,1}} \leq C \max_{1\leq j\leq N} \int_{t_{j-1}}^{t_j} \left\{1 + \frac{1}{\varepsilon}\exp\left(-\frac{\delta s}{\varepsilon}\right)\right\} ds, \tag{4.22}$$

while for the second case, i.e. on $\omega_{N,p}, 1 < p \leq m$, (4.21) and Lemma 4.1 gives

$$\|\mathcal{R}\|_{\omega_{N,p}} \leq C \max_{1\leq q\leq p} \max_{(q-1)N+1\leq j\leq qN} \int_{t_{j-1}}^{t_j} \left[1 + \left\{\frac{(s-r_{q-1})^{q-1}}{\varepsilon^q} + \frac{(s-r_{q-1})^{q-2}}{\varepsilon^{q-1}}\right\} \cdot \exp\left(-\frac{\delta(s-r_{q-1})}{\varepsilon}\right)\right] ds. \tag{4.23}$$

Afterwards, by the virtue of inequality $t^n e^{-t} \leq Ce^{-\beta t}$, $0 < \beta < 1$ and $t \in [0, \infty)$, we obtain the following expression from (4.23):

$$\|\mathcal{R}\|_{\omega_{N,p}} \leq C \max_{1\leq q\leq p} \max_{(q-1)N+1\leq j\leq qN} \int_{t_{j-1}}^{t_j} \left\{1 + \frac{1}{\varepsilon}\exp\left(-\frac{\delta(s-r_{q-1})}{\theta\varepsilon}\right)\right\} ds,\ \theta > 1,\ 1 < p \leq m. \tag{4.24}$$

On combining (4.22) and (4.24), we have

$$\|\mathcal{R}\|_{\omega_{N,p}} \leq C \max_{1\leq q\leq p} \max_{(q-1)N+1\leq j\leq qN} \int_{t_{j-1}}^{t_j} \left\{1 + \frac{1}{\varepsilon}\exp\left(-\frac{\delta(s-r_{q-1})}{\theta\varepsilon}\right)\right\} ds,\ \theta > 1,\ 1 \leq p \leq m.$$

Hence, using (4.17), the proof is completed. □

In order to tackle the layer behaviour of the solution of (4.1)–(4.2), below we consider some standard a priori meshes and deduce the convergence of the scheme using Theorem 4.1.

4.3.1 Shishkin meshes

For the discretization of problem (4.1)–(4.2), we construct a special piecewise-uniform mesh with the help of a transition parameter defined as

$$\sigma_q = r_{q-1} + \min\left\{\frac{r}{2}, \frac{\theta\varepsilon}{\delta}\ln N\right\}, \qquad 1 \le q \le m.$$

Thus, for an even integer N, the transition parameter σ_q partitions each sub-region $\mathfrak{I}_q$ into two segments $[r_{q-1}, \sigma_q]$ and $[\sigma_q, r_q]$ having equal number of mesh intervals. Note that for $\sigma_q = r_{q-1} + r/2$, ε is large and standard arguments could be used. So, we only discuss the case $\sigma_q = r_{q-1} + \theta\varepsilon \ln N/\delta$. It is easy to deduce that

$$\int_{t_{j-1}}^{t_j}\left\{1 + \frac{1}{\varepsilon}\exp\left(-\frac{\delta(s - r_{q-1})}{\theta\varepsilon}\right)\right\} ds \le C\left(h_j + \left|\exp\left(-\frac{\delta(t_{j-1} - r_{q-1})}{\theta\varepsilon}\right) - \exp\left(-\frac{\delta(t_j - r_{q-1})}{\theta\varepsilon}\right)\right|\right).$$

For $(q-1)N + 1 \le j \le (q-1)N + N/2$, we use mean value theorem for the second term and the bound $h_j \le C\varepsilon N^{-1}\ln N$ to get

$$\int_{t_{j-1}}^{t_j}\left\{1 + \frac{1}{\varepsilon}\exp\left(-\frac{\delta(s - r_{q-1})}{\theta\varepsilon}\right)\right\} ds \le CN^{-1}\ln N.$$

For $(q-1)N + N/2 + 1 \le j \le qN$, we use the value of σ_q to get

$$\int_{t_{j-1}}^{t_j}\left\{1 + \frac{1}{\varepsilon}\exp\left(-\frac{\delta(s - r_{q-1})}{\theta\varepsilon}\right)\right\} ds \le CN^{-1}.$$

Thus, (4.16) yields

$$||u - U||_{\bar{\omega}_{N_0}} \le CN^{-1}\ln N.$$

4.3.2 Bakhvalov meshes

These meshes are also a priori meshes, but usually they produce better results than Shishkin meshes, and are graded in nature. For the discretization of problem (4.1)–(4.2) although one can obtain these meshes by several means but we construct them by equidistribution of the following monitor function

$$M_B^q(t) := \max\left\{1, \frac{\mathcal{K}}{\varepsilon}\exp\left(-\frac{\delta(t-r_{q-1})}{\theta\varepsilon}\right)\right\},$$

where $\mathcal{K}$ is a positive constant chosen by the user. So, the mesh points on $\omega_{N,q}$ are chosen such that

$$\int_{t_{j-1}}^{t_j} M_B^q(s)ds = \frac{1}{N}\int_{r_{q-1}}^{r_q} M_B^q(s)ds.$$

Observing that $\int_{r_{q-1}}^{r_q} M_B^q(s)ds \leq C$, we get

$$\int_{t_{j-1}}^{t_j}\left\{1+\frac{1}{\varepsilon}\exp\left(-\frac{\delta(s-r_{q-1})}{\theta\varepsilon}\right)\right\}ds \leq CN^{-1}.$$

Consequently, (4.16) gives

$$||u-U||_{\bar{\omega}_{N_0}} \leq CN^{-1}.$$

4.4 A posteriori error analysis

In this section, we derive the a posteriori error estimate in the maximum norm for the discrete scheme (4.11)–(4.12). For this, we assume that $\widetilde{U}$ is the piecewise linear interpolant of the discrete solution $\{U_i\}_{i=1}^{N_0}$ on ω_{N_0}. Clearly, $\widetilde{U}$ is continuous on $\bar{\mathfrak{I}}$, linear on each sub-interval $[t_{i-1}, t_i]$, and at the mesh points it is equal to U_i, i.e. $\widetilde{U}(t_i) = U_i$. Further, for $t \in (t_{i-1}, t_i)$, we have the following equivalent definitions

for $\widetilde{U}$:

$$\widetilde{U}(t) = U_i + (t - t_i)D^- U_i \quad \text{and} \quad \widetilde{U}(t) = U_{i-1} + (t - t_{i-1})D^- U_i. \tag{4.25}$$

Thus, we have $\widetilde{U}'(t) = D^- U_i,\ t \in (t_{i-1}, t_i)$. Now we discuss the a posteriori error analysis of scheme (4.11)–(4.12) in the following theorem.

Theorem 4.2. *Let u and U be the solutions of (4.1)–(4.2) and (4.11)–(4.12) respectively, and $\widetilde{U}$ denotes the piecewise-linear interpolant of U. Then*

$$\left\|\widetilde{U} - u\right\|_\infty \le C_*\big(\lambda_1 + \lambda_2 + \lambda_3 + \lambda_4 + \lambda_5 + \lambda_6\big), \tag{4.26}$$

where $\lambda_j = \max\limits_{1\le i\le N_0} \lambda_{j,i}, j = 1, 2, \ldots, 6,$

$$\begin{aligned}
\lambda_{1,i} &:= \sum_{k=1}^{i-1} \left(\bar{K}_t |U_{k-1}| h_i + \bar{K}_s |U_{k-1}| h_k + \bar{L}_t |U_{k-N-1}| h_i + \bar{L}_s |U_{k-N-1}| h_k \right) h_k, \\
\lambda_{2,i} &:= \sum_{k=1}^{i-1} h_k^2 \bar{K} \left| D^- U_k \right| + h_i^2 \bar{K} \left| D^- U_i \right|, \\
\lambda_{3,i} &:= \sum_{k=1}^{i-1} h_k h_{k-N} \bar{L} \left| D^- U_{k-N} \right| + h_i h_{i-N} \bar{L} \left| D^- U_{i-N} \right|, \\
\lambda_{4,i} &:= 2\bar{K} h_i |U_{i-1}| + 2\bar{L} h_i |U_{i-N-1}|, \\
\lambda_{5,i} &:= \|f'\|_\infty h_i + \|a\|_\infty h_i \left| D^- U_i \right| + \|a'\|_\infty h_i |U_i| + \|a'\|_\infty h_i^2 \left| D^- U_i \right|, \\
\lambda_{6,i} &:= \|b\|_\infty h_{i-N} \left| D^- U_{i-N} \right| + \|b'\|_\infty h_i |U_{i-N}| + \|b'\|_\infty h_i h_{i-N} \left| D^- U_{i-N} \right|.
\end{aligned}$$

Proof. For any $t \in (t_{i-1}, t_i)$, we have

$$\begin{aligned}
&\mathscr{L}\widetilde{U}(t) - \mathscr{L}u(t) \\
&= \varepsilon \widetilde{U}'(t) + a(t)\widetilde{U}(t) + b(t)\widetilde{U}(t - r) + \int_0^t \left[K(t, s)\widetilde{U}(s) + L(t, s)\widetilde{U}(s - r) \right] ds - f(t) \\
&= \varepsilon D^- U_i + \left(a_i + \int_{t_i}^t a'(s)\, ds \right) \left(U_i + (t - t_i)D^- U_i \right)
\end{aligned}$$

$$
\begin{aligned}
&+\left(b_i+\int_{t_i}^{t}b'(s)\,ds\right)\left(U_{i-N}+(t-r-t_{i-N})D^-U_{i-N}\right)\\
&+\sum_{k=1}^{i-1}\int_{t_{k-1}}^{t_k}\left[K(t,s)\Big\{U_{k-1}+(s-t_{k-1})D^-U_k\Big\}+L(t,s)\Big\{U_{k-N-1}+(s-r-t_{k-N-1})D^-U_{k-N}\Big\}\right]ds\\
&+\int_{t_{i-1}}^{t}\left[K(t,s)\Big\{U_{i-1}+(s-t_{i-1})D^-U_i\Big\}+L(t,s)\Big\{U_{i-N-1}+(s-r-t_{i-N-1})D^-U_{i-N}\Big\}\right]ds\\
&-\left(f_i+\int_{t_i}^{t}f'(s)\,ds\right)\\
&=\varepsilon D^-U_i+a_iU_i+b_iU_{i-N}+\sum_{k=1}^{i}\int_{t_{k-1}}^{t_k}\Big[K(t_i,t_{k-1})U_{k-1}+L(t_i,t_{k-1})U_{k-N-1}\Big]\,ds-f_i\\
&+a_i(t-t_i)D^-U_i+U_i\int_{t_i}^{t}a'(s)\,ds+(t-t_i)D^-U_i\int_{t_i}^{t}a'(s)\,ds\\
&+b_i(t-r-t_{i-N})D^-U_{i-N}+U_{i-N}\int_{t_i}^{t}b'(s)\,ds+(t-r-t_{i-N})D^-U_{i-N}\int_{t_i}^{t}b'(s)\,ds\\
&+\sum_{k=1}^{i-1}\int_{t_{k-1}}^{t_k}\left[U_{k-1}\Big\{K(t,s)-K(t_i,t_{k-1})\Big\}+U_{k-N-1}\Big\{L(t,s)-L(t_i,t_{k-1})\Big\}\right]ds\\
&+\sum_{k=1}^{i-1}\int_{t_{k-1}}^{t_k}(s-t_{k-1})K(t,s)D^-U_k\,ds+\int_{t_{i-1}}^{t}(s-t_{i-1})K(t,s)D^-U_i\,ds\\
&+\sum_{k=1}^{i-1}\int_{t_{k-1}}^{t_k}(s-r-t_{k-N-1})L(t,s)D^-U_{k-N}\,ds+\int_{t_{i-1}}^{t}(s-r-t_{i-N-1})D^-U_{i-N}L(t,s)\,ds\\
&+U_{i-1}\left[\int_{t_{i-1}}^{t}K(t,s)\,ds-\int_{t_{i-1}}^{t_i}K(t_i,t_{i-1})\,ds\right]\\
&+U_{i-N-1}\left[\int_{t_{i-1}}^{t}L(t,s)\,ds-\int_{t_{i-1}}^{t_i}L(t_i,t_{i-1})\,ds\right]-\int_{t_i}^{t}f'(s)\,ds, \qquad (4.27)
\end{aligned}
$$

where we have used (4.25). Thus, using (4.11), we get

$$
\begin{aligned}
&\mathscr{L}\widetilde{U}(t)-\mathscr{L}u(t)\\
&=a_i(t-t_i)D^-U_i+U_i\int_{t_i}^{t}a'(s)\,ds+(t-t_i)D^-U_i\int_{t_i}^{t}a'(s)\,ds\\
&+b_i(t-r-t_{i-N})D^-U_{i-N}+U_{i-N}\int_{t_i}^{t}b'(s)\,ds+(t-r-t_{i-N})D^-U_{i-N}\int_{t_i}^{t}b'(s)\,ds\\
&+\sum_{k=1}^{i-1}\int_{t_{k-1}}^{t_k}\left[U_{k-1}\Big\{K(t,s)-K(t_i,t_{k-1})\Big\}+U_{k-N-1}\Big\{L(t,s)-L(t_i,t_{k-1})\Big\}\right]ds
\end{aligned}
$$

$$
\begin{aligned}
&+\sum_{k=1}^{i-1}\int_{t_{k-1}}^{t_k}(s-t_{k-1})K(t,s)D^-U_k\,ds+\int_{t_{i-1}}^{t}(s-t_{i-1})K(t,s)D^-U_i\,ds\\
&+\sum_{k=1}^{i-1}\int_{t_{k-1}}^{t_k}(s-r-t_{k-N-1})L(t,s)D^-U_{k-N}\,ds+\int_{t_{i-1}}^{t}(s-r-t_{i-N-1})D^-U_{i-N}L(t,s)\,ds\\
&+U_{i-1}\left[\int_{t_{i-1}}^{t}K(t,s)\,ds-\int_{t_{i-1}}^{t_i}K(t_i,t_{i-1})\,ds\right]\\
&+U_{i-N-1}\left[\int_{t_{i-1}}^{t}L(t,s)\,ds-\int_{t_{i-1}}^{t_i}L(t_i,t_{i-1})\,ds\right]-\int_{t_i}^{t}f'(s)\,ds. \qquad (4.28)
\end{aligned}
$$

Now we proceed as follows to evaluate each terms of (4.28) one by one. By Taylor expansions of $K(t,s)$ and $L(t,s)$ about (t_i,t_{k-1}), for some (η,ν) and $(\tilde{\eta},\tilde{\nu})$ in between (t,s) and (t_i,t_{k-1}), it holds

$$
\begin{aligned}
&\left|\sum_{k=1}^{i-1}\int_{t_{k-1}}^{t_k}\left[U_{k-1}\Big\{K(t,s)-K(t_i,t_{k-1})\Big\}+U_{k-N-1}\Big\{L(t,s)-L(t_i,t_{k-1})\Big\}\right]ds\right|\\
&\le\sum_{k=1}^{i-1}\Bigg|\int_{t_{k-1}}^{t_k}\Bigg[U_{k-1}\Big\{K(t_i,t_{k-1})+(t-t_i)K_t(\eta,\nu)+(s-t_{k-1})K_s(\eta,\nu)-K(t_i,t_{k-1})\Big\}\\
&+U_{k-N-1}\Big\{L(t_i,t_{k-1})+(t-t_i)L_t(\tilde{\eta},\tilde{\nu})+(s-t_{k-1})L_s(\tilde{\eta},\tilde{\nu})-L(t_i,t_{k-1}))\Big\}\Bigg]ds\Bigg|\\
&\le\sum_{k=1}^{i-1}\Big(\bar{K}_t|U_{k-1}|h_i+\bar{K}_s|U_{k-1}|h_k+\bar{L}_t|U_{k-N-1}|h_i+\bar{L}_s|U_{k-N-1}|h_k\Big)\int_{t_{k-1}}^{t_k}ds\\
&=\sum_{k=1}^{i-1}\Big(\bar{K}_t|U_{k-1}|h_i+\bar{K}_s|U_{k-1}|h_k+\bar{L}_t|U_{k-N-1}|h_i+\bar{L}_s|U_{k-N-1}|h_k\Big)h_k. \qquad (4.29)
\end{aligned}
$$

Now,

$$
\begin{aligned}
&\left|\sum_{k=1}^{i-1}\int_{t_{k-1}}^{t_k}(s-t_{k-1})K(t,s)D^-U_k\,ds+\int_{t_{i-1}}^{t}(s-t_{i-1})K(t,s)D^-U_i\,ds\right|\\
&\le\sum_{k=1}^{i-1}h_k\bar{K}\big|D^-U_k\big|\int_{t_{k-1}}^{t_k}ds+h_i\bar{K}\big|D^-U_i\big|\int_{t_{i-1}}^{t}ds\\
&\le\sum_{k=1}^{i-1}h_k^2\bar{K}\big|D^-U_k\big|+h_i^2\bar{K}\big|D^-U_i\big|. \qquad (4.30)
\end{aligned}
$$

Similarly, it follows that

$$\begin{aligned}&\left|\sum_{k=1}^{i-1}\int_{t_{k-1}}^{t_k}(s-r-t_{k-N-1})L(t,s)D^-U_{k-N}\,ds+\int_{t_{i-1}}^{t}(s-r-t_{i-N-1})L(t,s)D^-U_{i-N}\,ds\right|\\&\le\sum_{k=1}^{i-1}h_kh_{k-N}\bar{L}\big|D^-U_{k-N}\big|+h_ih_{i-N}\bar{L}\big|D^-U_{i-N}\big|.\end{aligned}\tag{4.31}$$

Next,

$$\begin{aligned}&\left|U_{i-1}\left[\int_{t_{i-1}}^{t}K(t,s)\,ds-\int_{t_{i-1}}^{t_i}K(t_i,t_{i-1})\,ds\right]\right|\\&\le\bar{K}|U_{i-1}|\left|\int_{t_{i-1}}^{t}ds+\int_{t_{i-1}}^{t_i}ds\right|\\&\le 2\bar{K}h_i|U_{i-1}|,\end{aligned}\tag{4.32}$$

$$\begin{aligned}&\left|U_{i-N-1}\left[\int_{t_{i-1}}^{t}L(t,s)\,ds-\int_{t_{i-1}}^{t_i}L(t_i,t_{i-1})\,ds\right]\right|\\&\le\bar{L}|U_{i-N-1}|\left|\int_{t_{i-1}}^{t}ds+\int_{t_{i-1}}^{t_i}ds\right|\\&\le 2\bar{L}h_i|U_{i-N-1}|.\end{aligned}\tag{4.33}$$

Finally

$$\begin{aligned}&\left|a_i(t-t_i)D^-U_i+U_i\int_{t_i}^{t}a'(s)\,ds+(t-t_i)D^-U_i\int_{t_i}^{t}a'(s)\,ds\right|\\&\le\big|a_i(t-t_i)D^-U_i\big|+\left|U_i\int_{t_i}^{t}a'(s)\,ds\right|+\left|(t-t_i)D^-U_i\int_{t_i}^{t}a'(s)\,ds\right|\\&\le\|a\|_\infty h_i\big|D^-U_i\big|+\|a'\|_\infty h_i|U_i|+\|a'\|_\infty h_i^2\big|D^-U_i\big|.\end{aligned}\tag{4.34}$$

$$\left|b_i(t-r-t_{i-N})D^-U_{i-N}+U_{i-N}\int_{t_i}^{t}b'(s)\,ds+(t-r-t_{i-N})D^-U_{i-N}\int_{t_i}^{t}b'(s)\,ds\right|$$

$$\leq \left|b_i(t-r-t_{i-N})D^-U_{i-N}\right| + \left|U_{i-N}\int_{t_i}^{t} b'(s)\,ds\right| + \left|(t-r-t_{i-N})D^-U_{i-N}\int_{t_i}^{t} b'(s)\,ds\right|$$

$$\leq \|b\|_\infty h_{i-N}\left|D^-U_{i-N}\right| + \|b'\|_\infty h_i|U_{i-N}| + \|b'\|_\infty h_i h_{i-N}\left|D^-U_{i-N}\right|. \tag{4.35}$$

Therefore, combining all these findings from (4.29)–(4.35) in (4.28), and using the inequality (4.5) we have the proof. □

4.5 Numerical results

In this section, we first describe the a posteriori mesh generation and then perform some numerical experiments. Further, a comparison of results on the a posteriori and a priori meshes is also given. Basically, the a posteriori mesh is dynamic in nature. Such meshes automatically improve at each iteration until it reaches a stopping criterion. The a posteriori estimates (4.26) derived in the previous section can underlie any reliable mesh-generation algorithm. However, we have implemented the adaptive mesh generation algorithm originally proposed by De Boor [40] in each sub-region $\omega_{N,q}$. For a discussion on the convergence of the algorithm, readers are suggested to see [43, 131]. Based on the a posteriori error estimate, an improved a posteriori mesh can be generated by solving the following weak equidistribution principle

$$\Psi_i \leq \frac{C_0}{N}\sum_{j=1}^{N}\Psi_j, \quad 1 \leq i \leq N,$$

where $C_0 > 1$ is a user-chosen constant and

$$\Psi_i := \lambda_{1,i} + \lambda_{2,i} + \lambda_{3,i} + \lambda_{4,i} + \lambda_{5,i} + \lambda_{6,i}.$$

We consider the following test examples for the numerical experimentation.

Algorithm 3: A posteriori mesh generation

Step 1. Set $q = 1$.

Step 2. Initially take a uniform mesh $\omega_{N,q}^{(k)} \equiv \left\{ t_q^{(k)} : t_{i,q}^{(k)} = i/N, (q-1)N \le i \le qN \right\}$ with $k = 0$.

Step 3. Compute the discrete solution $U_q^{(k)}$ satisfying (4.11)–(4.12) on the mesh $\omega_{N,q}^{(k)}$.

Step 4. Compute the discrete function $\Psi_{i,q}^{(k)}$ for $(q-1)N + 1 \le i \le qN$.

Step 5. Assign $\mathfrak{Q}_{i,q}^{(k)} = \sum_{j=(q-1)N+1}^{i} \Psi_{j,q}^{(k)}$. If

$$\max_{(q-1)N+1 \le i \le qN} \left\{ \Psi_{i,q}^{(k)} \right\} \le C_0 \mathfrak{Q}_{qN,q}^{(k)}/N \tag{4.36}$$

holds true for a user chosen constant $C_0 > 1$, then go to Step 7, else continue with Step 6.

Step 6. Set $U_{(q-1)N+i,q}^{(k)} = i\mathfrak{Q}_{qN,q}^{(k)}/N$, $0 \le i \le N$. Now, construct the mesh $\omega_{N,q}^{(k+1)} \equiv \{ t_q^{(k+1)} : t_{(q-1)N+i}^{(k+1)}, 0 \le i \le N \}$ by interpolating the point $\left(U_{(q-1)N+i,q}^{(k)}, t_{(q-1)N+i}^{(k+1)} \right)$ to $\left(\mathfrak{Q}_{(q-1)N+1+i,q}^{(k)}, t_{(q-1)N+i}^{(k)} \right)$ using the piecewise linear interpolation. Go to Step 3 and follow the procedure with $k = k + 1$.

Step 7. Declare $U_q^{(k)}$ as the solution on $\omega_{N,q}^{(k)}$. Next, we set $q = q + 1$ and proceed to Step 2 if $q \le m$.

Step 8. The final mesh is $\omega_{N_0} = \cup_{q=1}^{m} \omega_{N,q}^{(k)}$ and the solution is $U = \cup_{q=1}^{m} U_q^{(k)}$ on ω_{N_0}. Exit.

Example 4.1. *[103] Consider the problem*

$$\begin{cases} \varepsilon u'(t) + u(t) + u(t-1) + \displaystyle\int_0^t u(s-1)\, ds = 1, \quad t \in (0, 2], \\ u(t) = e^{-t}, \quad t \in [-1, 0]. \end{cases}$$

Example 4.2. *Consider the problem*

$$\begin{cases} \varepsilon u'(t) + (1+t)u(t) + t^2\cos(t)u(t-1) + \displaystyle\int_0^t [(s+t)u(s) + stu(s-1)]\,ds \\ \qquad\qquad = 5t^2 - 2\tanh(t), \quad t \in (0,2], \\ u(t) = 1 + te^{-t}, \quad t \in [-1,0]. \end{cases}$$

For Example 4.1, we have $a(t) = 1, b(t) = 1, K(t,s) = 0$ and $L(t,s) = 1$. Therefore, we have $\delta = 1$, $\|a\|_\infty = \|b\|_\infty = 1$, $\|a'\|_\infty = \|b'\|_\infty = \|f'\|_\infty = 0$, $\bar{K} = \bar{K}_t = \bar{K}_s = 0$, $\bar{L} = 1$, $\bar{L}_t = \bar{L}_s = 0$. For Example 4.2, we have $a(t) = 1+t, b(t) = t^2\cos(t), K(t,s) = s+t, L(t,s) = st$. Thus, we get $\delta = 1$, $\|a\|_\infty = 3, \|b\|_\infty = 4$, $\|a'\|_\infty = 1, \|b'\|_\infty = 8$, $\|f'\|_\infty = 19.86$, $\bar{K} = 4, \bar{K}_t = \bar{K}_s = 1$, $\bar{L} = 4$, $\bar{L}_t = \bar{L}_s = 2$. We solve the test examples for various values of N and ε, where $N \in S_N = \{2^{i+6}, i = 1, 2, \ldots, 7\}$ and $\varepsilon \in S_\varepsilon = \{10^{-i}, i = 0, 1, \cdots, 10\}$. The user chosen constant C_0 mentioned in the algorithm is precisely taken to be $C_0 = 1.2$ to construct the a posteriori mesh. For

$\varepsilon = 10^{-k}$	$N = 2^7$	$N = 2^8$	$N = 2^9$	$N = 2^{10}$	$N = 2^{11}$	$N = 2^{12}$	$N = 2^{13}$
$k = 0$	1.0238e-03	5.1577e-04	2.5885e-04	1.2967e-04	6.4894e-05	3.2462e-05	1.6235e-05
$k = 1$	1.1140e-02	5.5879e-03	2.7993e-03	1.4011e-03	7.0093e-04	3.5056e-04	1.7531e-04
$k = 2$	1.2396e-02	6.7922e-03	3.6247e-03	1.7766e-03	8.7814e-04	4.3638e-04	2.1750e-04
$k = 3$	1.5446e-02	7.3812e-03	4.2110e-03	2.1808e-03	1.1160e-03	5.5864e-04	2.8167e-04
$k = 4$	1.5981e-02	8.7443e-03	4.2845e-03	2.0522e-03	9.6164e-04	5.4010e-04	2.9198e-04
$k = 5$	1.8420e-02	8.4890e-03	4.4297e-03	2.3376e-03	1.1398e-03	5.5875e-04	2.7090e-04
$k = 6$	1.7374e-02	8.9529e-03	4.4305e-03	2.0629e-03	1.1766e-03	5.9278e-04	2.9271e-04
$k = 7$	1.8437e-02	8.9532e-03	4.6481e-03	2.3112e-03	1.1161e-03	5.4168e-04	2.9815e-04
$k = 8$	1.7998e-02	8.9532e-03	4.5924e-03	2.3191e-03	1.1768e-03	5.7925e-04	2.7101e-04
$k = 9$	1.8452e-02	9.1697e-03	4.6390e-03	2.3113e-03	1.1161e-03	5.9438e-04	2.9481e-04
$k = 10$	1.8218e-02	9.0852e-03	4.6373e-03	2.3513e-03	1.1685e-03	5.4167e-04	2.9815e-04
E^N	1.8452e-02	9.1697e-03	4.6481e-03	2.3513e-03	1.1768e-03	5.9438e-04	2.9815e-04
ρ^N	1.0089	0.9802	0.9832	0.9986	0.9854	0.9953	–

TABLE 4.1: Errors and rates of convergence using the a posteriori method for Example 4.1.

$\varepsilon = 10^{-k}$	$N = 2^7$	$N = 2^8$	$N = 2^9$	$N = 2^{10}$	$N = 2^{11}$	$N = 2^{12}$	$N = 2^{13}$
$k = 0$	2.6866e-03	1.3440e-03	6.7219e-04	3.3614e-04	1.6808e-04	8.4044e-05	4.2023e-05
$k = 1$	5.1685e-03	2.5840e-03	1.2919e-03	6.4590e-04	3.2294e-04	1.6147e-04	8.0733e-05
$k = 2$	1.1722e-02	6.1104e-03	3.1215e-03	1.5884e-03	8.0256e-04	4.0366e-04	2.0246e-04
$k = 3$	1.3557e-02	6.8167e-03	3.6861e-03	1.8985e-03	9.6614e-04	4.8719e-04	2.3622e-04
$k = 4$	1.3702e-02	7.1508e-03	3.8081e-03	1.8652e-03	9.8331e-04	5.0528e-04	2.5574e-04
$k = 5$	1.3826e-02	7.2965e-03	3.7835e-03	1.9581e-03	9.8977e-04	4.9736e-04	2.4404e-04
$k = 6$	1.2983e-02	6.8936e-03	3.8112e-03	1.8805e-03	9.9789e-04	5.1010e-04	2.3439e-04
$k = 7$	1.3518e-02	7.1945e-03	3.7911e-03	1.9641e-03	9.4514e-04	5.0478e-04	2.5771e-04
$k = 8$	1.3573e-02	7.2685e-03	3.8470e-03	1.9611e-03	1.0030e-03	4.7124e-04	2.1756e-04
$k = 9$	1.3497e-02	6.8594e-03	3.5634e-03	1.8473e-03	9.5509e-04	4.9252e-04	2.3366e-04
$k = 10$	1.3795e-02	7.1926e-03	3.7576e-03	1.8995e-03	9.7500e-04	4.9894e-04	2.4726e-04
E^N	1.3826e-02	7.2965e-03	3.8470e-03	1.9911e-03	1.0030e-03	5.1010e-04	2.5771e-04
ρ^N	0.9221	0.9235	0.9699	0.9695	0.9755	0.9850	–

TABLE 4.2: Errors and rates of convergence using the a posteriori method for Example 4.2.

Example 4.1 adding h_i to Ψ_i avoids mesh starvation [132]. As the exact solution for both examples is unavailable, we employ the double-mesh principle for evaluating the error. For this, we first compute the solution on the bisected mesh and then compare it with the solution obtained on the original mesh. In what follows next, we obtain the maximum pointwise errors by using

$$E^N_{\varepsilon,q} = \max_{t_i \in \omega_{N,q}} \left| U^N_{i,q} - U^{2N}_{i,q} \right|, \quad q = 1, 2,$$

where $U^N_{i,q}$ is the approximate solution on $\omega_{N,q}$ and $U^{2N}_{i,q}$ is the approximate solution when the mesh $\omega_{N,q}$ is bisected. We then compute $E^N_\varepsilon = \max_{q=1,2} E^N_{\varepsilon,q}$. To confirm the robustness of the proposed method, we also evaluate the uniform error $E^N = \max_{\varepsilon \in S_\varepsilon} E^N_\varepsilon$ corresponding to each value of $N \in S_N$. Moreover, the parameter robust

Mesh	$N = 2^7$	$N = 2^8$	$N = 2^9$	$N = 2^{10}$	$N = 2^{11}$	$N = 2^{12}$	$N = 2^{13}$
A posteriori mesh	1.8452e-02	9.1697e-03	4.6481e-03	2.3513e-03	1.1768e-03	5.9438e-04	2.9815e-04
	1.0089	0.9802	0.9832	0.9986	0.9854	0.9953	–
Shishkin mesh	2.7402e-02	1.4719e-02	8.3358e-03	4.6470e-03	2.5596e-03	1.3966e-03	7.5633e-04
	0.8967	0.8203	0.8430	0.8604	0.8739	0.8849	–
Bakhvalov mesh	1.9792e-02	1.0016e-02	5.0386e-03	2.5270e-03	1.2655e-03	6.3322e-04	3.1673e-04
	0.9825	0.9913	0.9956	0.9979	0.9989	0.9994	–

TABLE 4.3: Comparison of parameter robust errors E^N and convergence orders ρ^N for Example 4.1.

rate of convergence is obtained by using

$$\rho^N = \log_2 \left(\frac{E^N}{E^{2N}} \right).$$

In Tables 4.1 and 4.2, we provide numerical results on a posteriori meshes for

Mesh	$N = 2^7$	$N = 2^8$	$N = 2^9$	$N = 2^{10}$	$N = 2^{11}$	$N = 2^{12}$	$N = 2^{13}$
A posteriori mesh	1.3826e-02	7.2965e-03	3.8470e-03	1.9911e-03	1.0030e-03	5.1010e-04	2.5771e-04
	0.9221	0.9235	0.9699	0.9695	0.9755	0.9850	–
Shishkin mesh	1.3883e-02	8.2750e-03	4.7713e-03	2.6892e-03	1.4913e-03	8.1720e-04	4.4378e-04
	0.7464	0.7944	0.8272	0.8507	0.8678	0.8808	–
Bakhvalov mesh	1.1027e-02	5.4797e-03	2.7314e-03	1.3636e-03	6.8127e-04	3.4050e-04	1.7022e-04
	1.0089	1.0044	1.0022	1.0011	1.0006	1.0003	–

TABLE 4.4: Comparison of parameter robust errors E^N and convergence orders ρ^N for Example 4.2.

Examples 4.1 and 4.2, respectively. The last two rows of these tables represent the uniform errors and the uniform rates of convergence. It is clear from these tables that the proposed method is parameter uniformly convergent of order $O(N^{-1})$. Apart from the a posteriori mesh, we have also implemented the discrete scheme on the a priori meshes, viz., Bakhvalov and Shishkin meshes for Examples 4.1 & 4.2, and the corresponding results are displayed in Tables 4.3 & 4.4, respectively. Here, the Shishkin mesh is constructed with $\theta = 1.1$ for both examples. The results on a posteriori mesh are better than the results on the Shishkin mesh. The results are

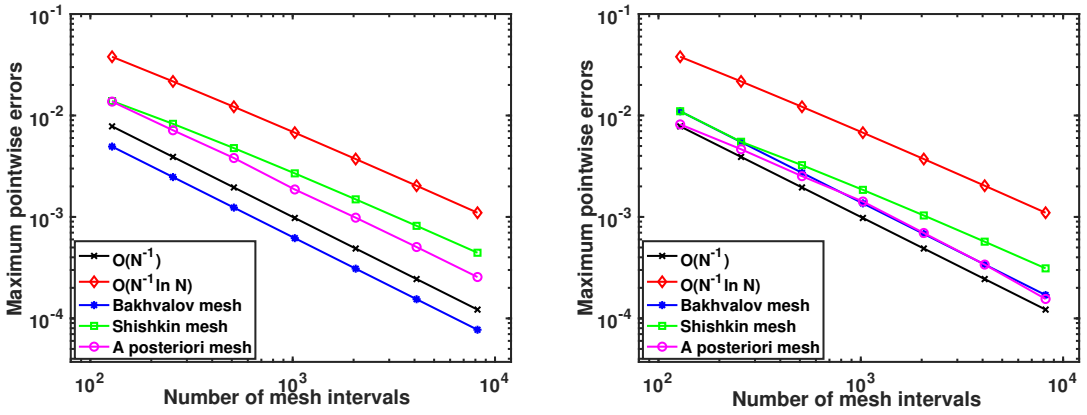

(A) On the interval $[0, 1]$ (B) On the interval $[1, 2]$

FIGURE 4.1: Log-log plots for Example 4.2 with $\varepsilon = 10^{-4}$.

similar for a posteriori and Bakhvalov meshes, but to generate the Bakhvalov mesh we need a priori information about the solution behaviour; more precisely, we need to know the locations and sizes of the layers present in the solution. While, the a posteriori mesh generation does not require any a priori information.

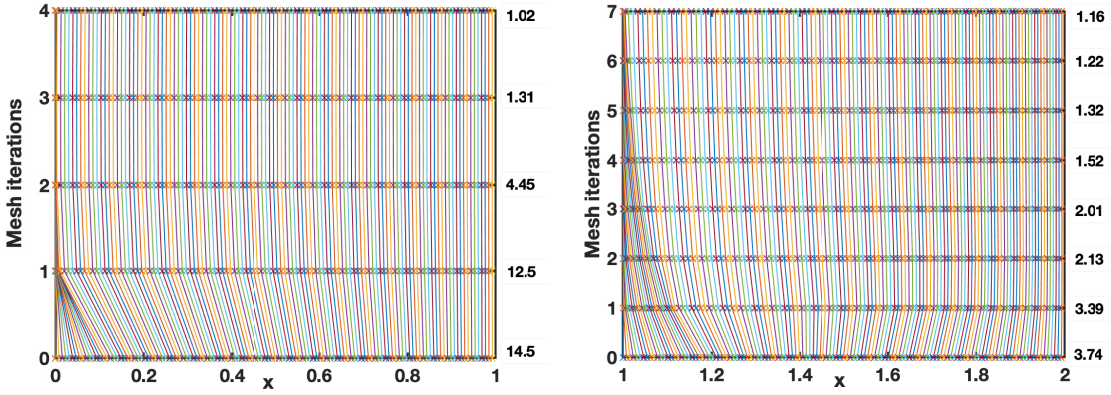

(A) On the interval $[0, 1]$ (B) On the interval $[1, 2]$

FIGURE 4.2: A posteriori mesh movements for Example 4.2 with $N = 128$ and $\varepsilon = 10^{-4}$.

In order to verify the rates of convergence graphically on each meshes, for Example 4.2, we provide the log-log graphs of maximum pointwise error vs. N in Figure 4.1 with $\varepsilon = 10^{-4}$. For a better understanding of how the a posteriori grids automatically detects the layer, for Example 4.2, we have plotted mesh iterations vs. t graph for

each sub-region in Figure 4.2 taking $N = 128$ and $\varepsilon = 10^{-4}$. Observe that it takes very few iterations to reach the stopping criterion and thus saves the computational cost. After each iterations, more and more number of mesh points condenses towards the left end-point of each sub-region which concludes that the solution has layers near $t = 0$ and $t = 1$. This graph also shows that the a posteriori mesh is truly adaptive in nature. Additionally, we plot the solution graph in Figure 4.3 for Example 4.2 with fixed N but varying ε. This figure reveals that as the perturbation parameter ε becomes smaller, the layer region at $t = 0$ and $t = 1$ gets thinner.

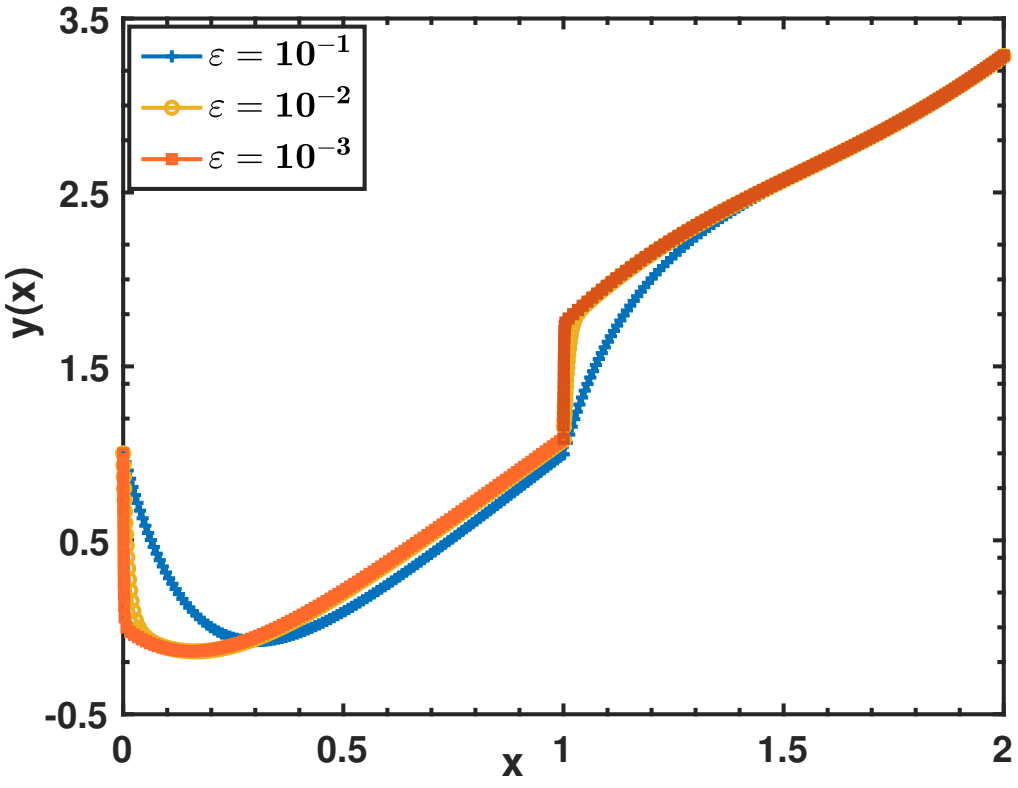

FIGURE 4.3: Solution plot for different values of ε with $N = 128$ for Example 4.2.

4.6 Conclusions

A first-order linear singularly perturbed delay Volterra integro-differential equation is considered that exhibits multiple layer phenomena. The discretization consists of an implicit difference scheme for the derivative term and a composite numerical integration rule for the integral term. A priori and a posteriori error analysis for the proposed discrete scheme is carried out. Numerical experiments are conducted which support the theory.